ACS Photonics

pubs.acs.org/journal/apchd5

Letter

Ultrafast Wavefront Shaping via Space-Time Refraction

Qingyuan Fan,[○] Amr M. Shaltout,[○] Jorik van de Groep, Mark L. Brongersma, and Aaron M. Lindenberg*

Cite This: https://doi.org/10.1021/acsphotonics.3c00498

Read Online

ACCESS | Metrics & More | Article Recommendations | Supporting Information

ABSTRACT: A myriad of metasurfaces have been demonstrated that manipulate light by spatially structuring thin optical layers. Manipulation of the optical properties of such layers in both space and time can unlock new physical phenomena and enable new optical devices. Examples include photon acceleration and frequency conversion, which modifies Snell's relation to a more general, nonreciprocal form. Here, we combine theory and experiment to realize wavefront shaping and frequency conversion on subpicosecond time-scales by inducing space-time refractive index gradients in epsilon-near-zero (ENZ) films with femtosecond light pulses. We experimentally tune wavefront steering by controlling the incident angle of the beams and the pump−probe delay without the need for nanostructure fabrication. As a demonstration of this approach, we leverage the ultrafast, high-bandwidth optical response of transparent oxides in their ENZ wavelength range to create large refractive index gradients and new types of nonreciprocal, ultrafast two-dimensional (2D) optics, including an ultrathin transient lens.

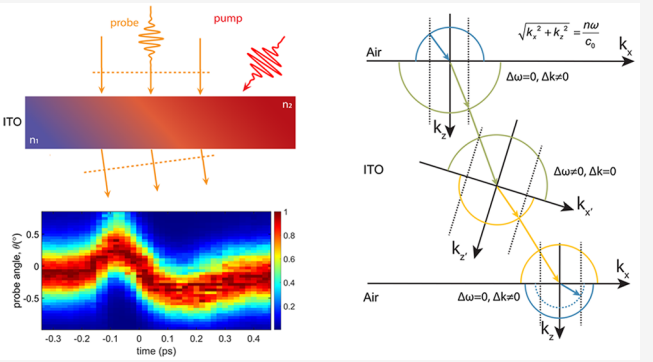

KEYWORDS: *epsilon-near-zero, ultrafast optics, space-time refraction*

1. INTRODUCTION

Photonic metasurfaces[1−4] have radically changed the way we engineer light−matter interactions and have taught us how to spatially structure materials at a subwavelength scale to induce space-variant phase-shifts. Consequently, photons propagating through a metasurface can undergo changes in their momentum, angular-momentum, and spin state. This has led to a generalization of Snell's law,[2] a fundamental relation in optics, and has enabled an entirely new family of 2D optical elements, including flat lenses,[5] holograms,[6] and wave-plates.[7] The similarity of space and time in Maxwell's equations suggests that further structuring of materials in the time-domain can enable new physical phenomena and broaden the range of applications.[8] Therefore, temporally engineered materials created by electrical,[9−13] mechanical,[14] and optical modulation[13,15,16] have gained recent attention. Light propagating through time-variant metasurfaces undergoes time-refraction-based frequency conversion[8,17−24] and time reversal,[25] which modifies Snell's relation to an even more general nonreciprocal form.[26−29] Recent research on ENZ materials has demonstrated large refractive index modulation, which enables large frequency-shifts at subpicosecond time-scales.[30−32] Certain transparent conducting oxides (TCOs) possess ENZ characteristics in the near-IR wavelength range. For this reason, they can serve as an excellent material platform to demonstrate the nonreciprocal form of Snell's law as well as to realize ultrafast wavefront shaping with space-time refracting optics.

In this paper, we capitalize on the generalized Snell's law to theoretically and experimentally investigate ultrafast beam deflection by transiently inducing a refractive index gradient in an indium tin oxide (ITO) film, which dynamically evolves in space and time. The probe wavelengths are in the ENZ region, where the real part of the permittivity is close to zero, contributing to a large nonlinearity.[30] We demonstrate a nonreciprocal, all-optical wavefront shaping method in the optical communication wavelength range, enabling pump−probe angle-dependent beam deflection, operating even under normal-incidence illumination conditions. We verify that the deflection amplitude is maximized in the ENZ wavelength range, where the nonlinearity is maximized. The role that the pump−probe angle plays in beam steering is also studied. The wavefront deflection magnitude is found to be nearly proportional to the angle between the pump and probe beams for small angles. We use this approach to demonstrate

Received: April 14, 2023

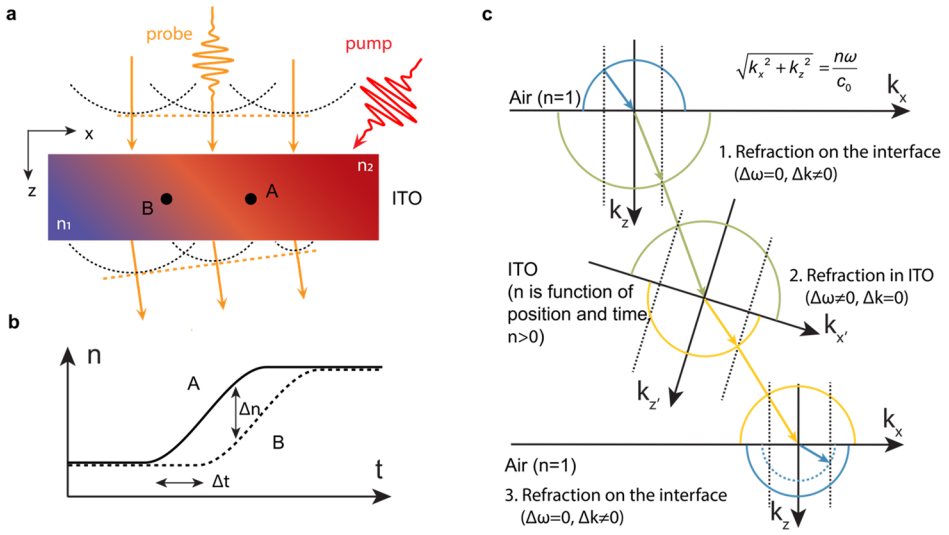

Figure 1. Space-time refraction. (a) The space-variant refractive index induced by a pump pulse is indicated by color with n_1 (blue) and n_2 (red) defining the indices before and after pump, respectively. A normal-incident probe beam (orange) is deflected away from the pump beam (red) direction when $n_1 < n_2$. The black and orange dashed lines indicate the envelopes of the point sources and wavefronts of the probe beam according to Huygens' principle. (b) Time-variant refractive index at different locations in space (A and B in (a)). Assuming an equal pump fluence at the locations, A and B have the same temporally varying index with a time delay. The difference of the refractive index at a point in time between A and B induces the space-variant refractive index in (a). (c) Iso-frequency contour of momentum. The momentum must point from the center to a point on the isofrequency contour or in a reverse direction. The radius of the contour is determined by the frequency and the refractive index of the material ($k = n\omega/c_0$). The black dashed lines are equally spaced from the k_z and $k_{z'}$ axes, which enforce momentum conservation in the tangential direction. This demonstrates the space-time refraction process, including the refraction that occurs at the air−ITO interfaces (processes 1 and 3) as well as the refraction with space-time-variant index in ITO (process 2; shown for an assumed increase in index and a frequency redshift).

an ultrafast, flat-optic lens with a focal length of 101 mm. While the beam focusing function may initially appear similar to the Kerr-induced self-focusing effect, our research employs a distinct mechanism to induce a spatial gradient of the refractive index. This index gradient is dependent on the local incident angle of the pump, which we show facilitates other functionalities using a designed incident pump beam.

2. PRINCIPLE OF SPACE-TIME REFRACTION IN AN ENZ FILM

It is known both theoretically and experimentally that the frequency of photons can be shifted when they propagate in a material with a temporally varying refractive index.[20,22,33,34] The frequency shift can be expressed as

$$\delta\omega = -\frac{\omega}{n_g}\delta n \tag{1}$$

where n_g is the group index of the material.

We find here that the fast refractive index modulation also makes ultrafast wavefront steering possible by inducing spatial gradients in the refractive index. In a general form, the spatiotemporal gradient that the pump induces in the ITO modifies Snell's law for the probe as follows:[26,35−37]

$$k_t \sin\theta_t = k_i \sin\theta_i + \frac{\partial\varphi}{\partial x} \tag{2}$$

where $k_i = \omega_i/c$ and $k_t = \omega_t/c$ are the wavenumbers of the incident and transmitted probe beams, and $\frac{\partial\varphi}{\partial x}$ is the spatial gradient of the phase-shift imparted onto the probe beam along the ITO surface. Equation 2 highlights that two underlying mechanisms that cause deflections of the probe angle from the conventional Snell's relation: (1) The space-gradient term, $\frac{\partial\varphi}{\partial x}$; (2) The frequency shift $\delta\omega$ discussed by eq 1 and the associated change in wave vector k_t induced by the time-gradient, which causes modification to θ_t. The impact of both space- and time-gradient effects is discussed in more detail in the following sections.

The first mechanism of beam wavefront shaping arises from a spatial gradient of the refractive index, which is demonstrated in Figure 1a,b. Upon photoexcitation, hot carriers are created that induce a dynamically varying refractive index, $n(t)$, which is changing at a rate $\frac{\partial n}{\partial t}(t)$.[30] We will describe the optical measurements and modeling to quantify this rate later in the manuscript. Assuming a pump pulse with a planar wavefront traveling through the material with a group velocity of $v_{g(pump)}$, different locations are excited at different time delays $\Delta\tau$, experiencing temporal index change $n(t + \Delta\tau)$. Two locations with a space interval of $\Delta z'$ in the pump propagation direction are separated by a time interval $\Delta\tau = \Delta z'/v_g$. A spatial gradient in the refractive index is established (Figure 1b), with magnitude:

$$\nabla n = \frac{\partial n}{\partial z'} = \frac{\partial n}{\partial t}\cdot\frac{\partial t}{\partial z'} = \frac{1}{v_{g(pump)}}\frac{\partial n}{\partial t} \tag{3}$$

The spatial gradient ∇n induces the phase gradient $\partial\phi/\partial x$ term, as indicated in eq 2, which is proportional to the projection of the spatial gradient along the film surface $\partial n/\partial x$.[15] When the steering magnitude is small, the angular shift can be written in a straightforward form:

$$\delta\theta_{probe} \approx \sin\delta\theta_{probe} = \frac{|\nabla n|}{n_0}\sin(\theta_{pp})\delta l = \frac{1}{v_{g(pump)}}\frac{1}{n_0}\frac{\partial n}{\partial t}\sin(\theta_{pp})\delta l \tag{4}$$

where $\delta l = \delta z/\cos(\theta_{probe})$ is the distance that the probe beam propagates and θ_{pp} is the local angle between pump and probe propagating directions. A more general form of the wavefront steering equation and details of the derivation are discussed in

https://doi.org/10.1021/acsphotonics.3c00498
ACS Photonics XXXX, XXX, XXX−XXX

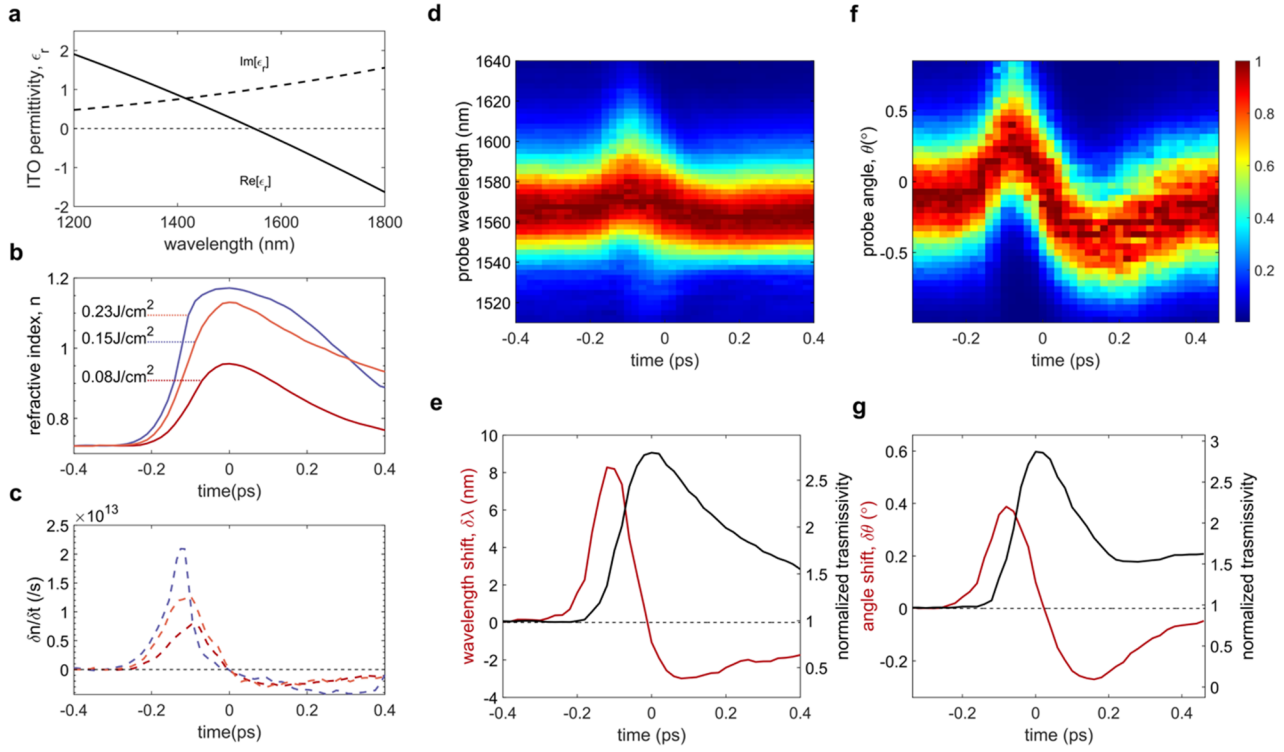

Figure 2. Ultrafast modulation of the frequency and direction of an optical beam. (a) Static wavelength-dependent permittivity. (b) Transient refractive index (real part) at 1540 nm. (c) The rate of change of the index, dn/dt, with different pump fluences at 1540 nm. (d) Normalized transient spectrum and (e) integrated transmissivity (black) and central wavelength (red) as a function of pump−probe delay, measured at a pump fluence of 0.23 J/cm^2. (f) Normalized transient distribution in the angular direction. (g) Integrative transmissivity (black) and central deflection angle (red) as a function of pump−probe delay, with a pump fluence of 0.31J/cm^2. In (d)−(g), the incident angle of the probe beam is 20°, and the pump beam is normally incident.

the Supporting Information. By the integration of eq 4 along the path of the probe beam, the deflection angle can be determined. In the context of this study employing the ITO film platform, the film thickness is on the order of micrometers and the photon propagation time is approximately 10 fs, which is short compared with the time scale of index change. These values suggest minimal variations in the parameters outlined in eq 4, including θ_{pp}, $\partial n/\partial t$, n_0 and $v_{g(pump)}$. Consequently, these parameters can be treated as constants, enabling simplification of the integral for calculating the deflection angle using the following equation:

$$\Delta\theta = \int_l \delta\theta_{probe} \approx \Delta l \frac{1}{v_{g(pump)}} \frac{1}{n_0} \frac{\partial n}{\partial t} \sin(\theta_{pp}) \tag{5}$$

In addition to spatial gradients, the temporal gradient in the refractive index also induces a frequency shift that contributes to the beam deflection. Refraction occurs at the interfaces between the air and ITO film (processes 1 and 3 in Figure 1c), as well as on virtual interfaces inside the ITO, which are iso-index planes generated by the spatial gradient of the index (process 2 in Figure 1c). In both cases, conservation of momentum holds for tangential directions, so the momentum of both the incident and refracted beams have equal projections along the x or x' directions, at the start and end of the black dashed lines. The wavefront steering $\delta\theta_{probe}$ from the spatial gradient in the film is demonstrated in process 2 in Figure 1c. As mentioned by eq 1, the frequency of the probe pulses is shifted with temporally varying refractive index, which does not break the in-plane conservation of momentum ($\delta k = \delta\left[n(\omega)\cdot\frac{\omega}{c}\right] = 0$), and as a result, the temporal gradients of index do not contribute to beam deflection inside ITO. However, the deflection from temporal gradients appears upon the refraction from ITO into the air, where frequency conversion $\Delta\omega$ imparted from time-variant index induces a momentum shift $\Delta k=\Delta\omega/c_0$. In the last iso-frequency contour of process 3 in Figure 1c, the momentum of the refracted beam ends on the blue dashed contour, which has a radius difference Δk with the original wavevector indicated by the blue solid contour. The Δk from the frequency conversion also contributes to the beam deflection. The difference of the refraction angle from the solid iso-frequency contour to the dashed contour in process 3 indicates the contribution of the wavefront steering from a frequency shift generated by temporal index modulation.

In special conditions when the pump beam is normally incident, it generates spatial gradients of the index perpendicular to the ITO-air interface. With a given incident angle θ_{probe}, an angular frequency ω, and an accumulated frequency shift through the medium $\Delta\omega$, an optical beam will be deflected by

$$\Delta\theta_{probe} = \arcsin\left(\frac{\omega}{\omega + \Delta\omega}\cdot\sin(\theta_{probe})\right) - \theta_{probe} \tag{6}$$

The total beam deflection therefore results from both the transverse spatial index gradient and the time-varying index, as indicated by eqs 4 and 6.

This beam deflection contributed from the temporal gradient of refractive index is nonreciprocal. This effect occurs

https://doi.org/10.1021/acsphotonics.3c00498
ACS Photonics XXXX, XXX, XXX−XXX

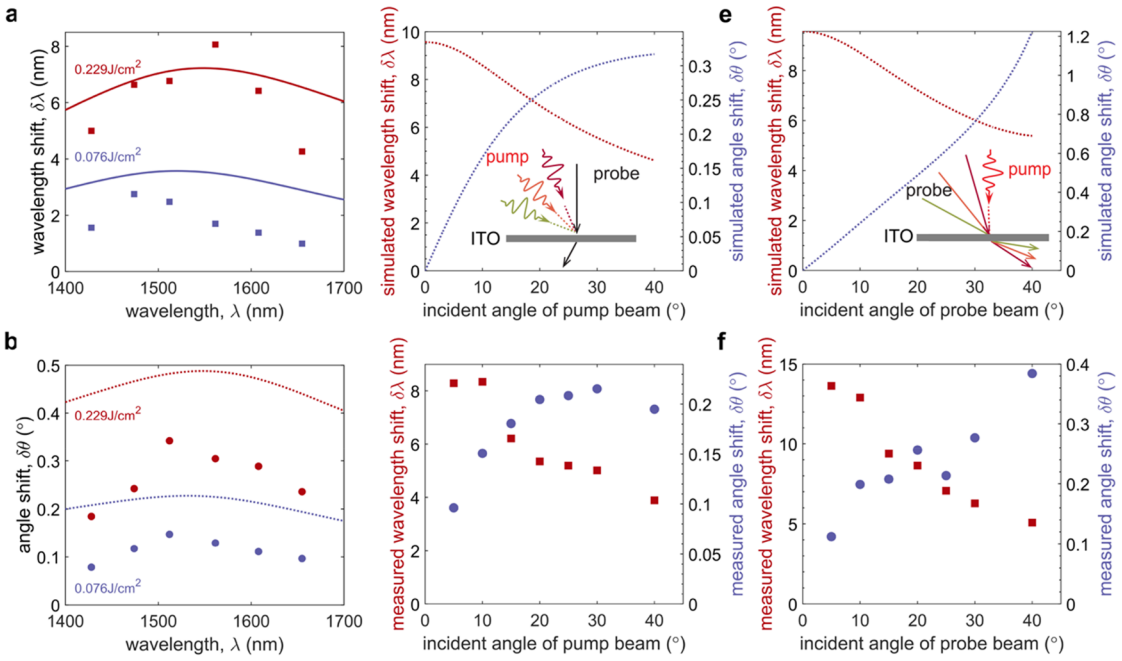

Figure 3. Wavelength and incidence angle dependence. (a) Simulated and measured probe wavelength-dependent wavelength shift and (b) angle shift at fluences of 0.08 and 0.23 J/cm^2, pumping at normal-incidence and probing at 15°. (c) Simulated and (d) measured wavelength and angle shift as a function of the incident angle of the pump when the probe is at normal incidence. (e) Simulated and (f) measured wavelength and angle shift as a function of the incident angle of the probe, while the pump is directed at normal incidence.

when the variation in the refractive index induced by pump pulses disrupts the time symmetry of the system. Specifically, considering a scenario with an increasing refractive index, a probe pulse propagating through the pumped ITO-film system experiences a redshift in frequency and an increase in refraction angle. A beam propagating in the opposite direction accumulates additional redshift and refraction angle increase, rather than exhibiting propagation opposite to the incident direction, which make the temporal deflection process nonreciprocal.

3. RESULTS

3.1. Experimental and Simulation Study on the Transient Beam Deflection. The experiments are conducted on ITO, which is a common transparent conductive oxide following a Drude-metal-like optical behavior with a real permittivity close to zero at near-infrared wavelengths, tunable by doping.[38] The sample is a commercially obtained 800 nm thick ITO film grown by CVD on a quartz substrate. After cleaning, the sample is annealed in a forming gas atmosphere at 300 °C for 18 min to tune the ENZ condition to $\lambda \approx 1550$ nm. Optical pulses at 800 nm and of 55 fs pulse duration are generated by a Ti:sapphire amplifier at a 1 kHz repetition rate, and an optical parametric amplifier is used to generate the probe pulse in the ENZ region (see details in the Supporting Information).

The static and dynamic optical properties of the material are first characterized. The static permittivity is first calculated by measuring the transmissivity $T(\lambda)$ and reflectivity $R(\lambda)$ (shown in Supporting Information Figure S2) at multiple incident angles and polarization with the setup as shown in Figure S1. The experimental data are used to fit to a Drude model as the dielectric function using the transfer matrix method. The results indicate that the real part of the permittivity ϵ_r' vanishes at 1548 nm (Figure 2a). The ITO sample is then pumped with 800 nm pulses at different fluences, and the transient transmissivity $T(\lambda,t)$ and reflectivity $R(\lambda,t)$ are measured. These measurements are then used to calculate the time-dependent Drude parameters. The transient index $n(t)$ and its rate of change $dn(t)/dt$ at 1540 nm are plotted in Figure 2b,c. The peak temporal gradient of index occurs at the rising edge of the transient transmission curve, where the strongest space-time refraction is predicted to occur. The dynamic characteristics of the imaginary part of the refractive index exert an influence on the absorption and transmissivity of the probe beam yet do not contribute to the frequency and deflection angle shift. The characterization and calculation of the imaginary of the index are in the Supporting Information.

The frequency conversion of the transmitted probe beam is measured with a spectrometer. The probe beam is also sent to the photodiode, which is scanned along the transverse direction of the probe beam to map its angular distribution. With a probe beam incident at 20°, a transmissivity of 4% is measured. By applying a normally incident pump beam, the transient transmissivities are observed, with the rising and decaying slopes corresponding with the modulation and recovery of the refractive index (Figure 2e–g). A red-shift and increase in the refraction angle are observed at the rising slope of the transmissivity, as shown in Figure 2d–g. This matches the calculations from eqs 5 and 6 when the refractive index is increased. Both the frequency conversion and the deflection angle have maximum amplitudes at a time delay for which the rate of change in the refractive index is largest, as expected. The probe wavelength is tuned using an optical parametric amplifier from ~1400 to ~1700 nm. Simulated and measured results both show maximum results near the probe wavelength of 1548 nm. The wavelength dependent results verify that the frequency and angle shift effects are enhanced at the ENZ wavelength because of the vanishing real permittivity and large relative index change $\Delta n/n$ (Figure 3a,b).

https://doi.org/10.1021/acsphotonics.3c00498
ACS Photonics XXXX, XXX, XXX−XXX

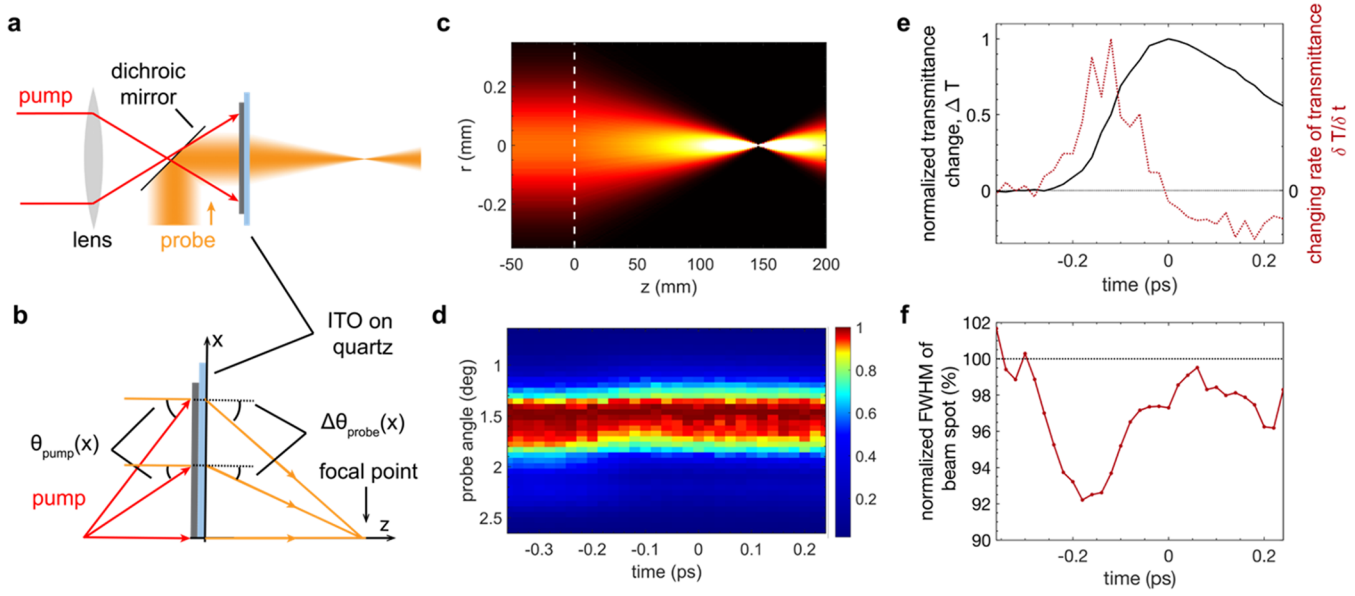

Figure 4. A transient ultrafast lens. (a) Setup diagram: The pump beam is focused upstream of the sample by a lens and becomes divergent on the ITO film. (b) Ray diagram. Incident angle of the pump beam is zero in the center of the beam spot and increases along the radius direction, which deflects the probe beam with larger angle. The probe beam is focused on one spot on the optical axis. (c) Simulated light intensity mapping of a 1540 nm beam undergoing focusing: a pump beam with a fluence of 0.23 J/cm^2 is focused 3 mm from the sample (at the white dashed line). A perfectly collimated Gaussian probe beam is assumed (fwhm = 30 μm). No small angle or paraxial approximation is used in the simulation. The transient behavior of the effective lens in (c) is experimentally studied by detecting the focusing of a divergent probe beam. (d) Normalized angular distribution of the probe beam as a function of pump−probe delay. (e) The transmissivity change (ΔT, black) and changing rate of the transmissivity ($\delta T/\delta t$, red). (f) The beam spot size (full width at half of maximum) of the probe beam spot as a function of pump−probe delay is plotted, with a maximum effect of focusing at the pump−probe delay for which the rate of change in the index is maximized.

As noted, both spatial and temporal index gradients contribute to beam deflection. To separate the two mechanisms, we experimentally verify the response in two experimental conditions: (1) probe normally and pump at various angles (Figure 3c,d), where the effect of the time-varying index is negligible, and (2) pump normally and probe at various angles (Figure 3e,f), where the spatial index gradient is zero along the sample surface. It is predicted by the cosine term in eq 3 that a large pump−probe angle enables a stronger space-time refraction because of a larger projection of the spatial index gradient on the transverse direction of the probe beam. A larger incident angle of the probe beam also increases the frequency conversion and deflection angle, as it provides a longer propagating length and light-matter interaction time in the ITO film. The experimental results of the deflection angle fit the expectation above, in positive correlation with the pump−probe angle. Additional interesting phenomena that are not covered by eqs 4 and 6 are also observed: in the experiments, a decreasing frequency shift is observed at larger incidence angles, with a saturation and decrease of probe angle deflection in the case of a normally incident probe (Figure 3d,f). This can be understood from the fact that the probe pulse has a finite spatial profile with a spatial photon distribution. At an off-normal incident angle, photons in a pulse arrive at the ITO surface with different pump−probe delays, lowering the averaged frequency shift and deflection angle. Taking this averaging effect into consideration with measured probe beam width (35 μm) and a pulse duration (55 fs), simulation of both frequency conversion and beam deflection matches the experimental results well (Figure 3c,e). A wavefront steering of 0.4° and frequency conversion of 14 nm is observed.

3.2. Realization of an Ultrathin Transient Lens.

Ultrafast wavefront shaping defines novel opportunities to manipulate light. Bending wavefronts with spatial gradients of the refractive index is utilized in self-focusing, which has been investigated since the 1960s.[39−41] This effect is generally realized using weak $\chi^{(3)}$ effects and detectable only when accumulated over a long distance. Operation near the ENZ frequency in ITO enables the observation of this effect in thin films. In self-focusing or beam deflection with nonlinear refraction, the spatial gradient of the index in nonlinear materials is induced by an intensity gradient of the beam spot, usually with a Gaussian-like transverse profile. However, this approach typically does not support more complex wavefront structuring. Here we show how the incident angle and pump−probe delay-controlled wavefront shaping can enable additional more complex dynamic 2D optics including the transient induction of an ultrafast lens. A focused pump pulse is divergent after the focal point with increasing incident angles from the beam center to the edge (Figure 4a,b). As the deflection amplitude is proportional to the sine of the angle between the pump and probe $\sin(\theta_{pp})$, as indicated in eq 4, the ITO film functions as an ultrafast lens to focus light. Within a small angle approximation and paraxial approximation, rays in the probe beam at different distance from the axis r will be focused to a spot, with a focal length (details in the Supporting Information) of

$$f(r, t) \approx \frac{n(t) z_0 v_{g(pump)}}{\frac{\partial n}{\partial t}(t) \cdot L} \tag{7}$$

which is, critically, independent of the radius r, thus enabling focusing with minimal off-axis aberrations. We simulate the light intensity distribution with ultrafast focusing for the case of

https://doi.org/10.1021/acsphotonics.3c00498
ACS Photonics XXXX, XXX, XXX−XXX

a 1540 nm probe beam focused by a pump beam with fluence of 0.23 J/cm^2 at a spot 3 mm before the sample (Figure 4c). The results show that the probe beam is focused 147 mm away, with a small spherical aberration. The ultrafast lensing effect is also verified by experiments, with the same pump conditions as in Figure 4c. Limited by the size of the sample, a slightly divergent probe beam is used. The beam spot width after the ITO film is observed to transiently contract (Figure 4d,f), consistent with an expected positive lens. As expected, this beam focusing effect is maximized at the rising edge of transient transmittance, which is the pump−probe delay with the largest index changing rate consistent with eq 5 (Figure 4e,f). We note that the beam spot size (full width at half-maximum, fwhm) is also influenced by the transient transmittance, because our pump intensity is not perfectly uniform, with a higher fluence in the center. A fwhm contraction of the beam spot contributed by the nonuniformity of pump intensity can be seen at $t = 0$ in Figure 4f, where the changing rate of index (Figure 4e, red) is zero and induces zero beam focusing effect. Because this effect arises from the uniform transmittance change, by subtracting the influence of the transient transmittance change, a 5.9% reduction in the beam spot size due to the focusing action with time leads to an estimated ultrafast lens with a focal length of 101 mm, in reasonable agreement with the theoretical estimated value. In the simulation, the transient refractive index change process with a normally occurring pump beam is used to calculate the beam deflection. However, at the outer part of the pump beam spot, at an oblique incident angle, the nonlinearity may be larger than at normal-incidence,[30] which results in a larger focusing effect. This indicates a possible reason that the simulation underestimates the focusing effect of the ultrafast thin lens compared to the experimental results.

4. CONCLUSION

In conclusion, we use the space-time refraction of light to mold the flow of an optical beam, dynamically controlling its direction and additionally realizing a transient lensing effect. Ultrafast wavefront shaping with spatiotemporal refraction is achieved by inducing refractive index gradients that develop within 100 fs and recover on subpicosecond time scales. The rapid subpicosecond index recovery may enable the construction of photonic time crystals (PTCs) or other time structures,[42−44] unveiling new physical phenomena and applications. The phenomenon is strongly enhanced near the ENZ wavelength because of the increased nonlinear material response. Two processes enable control of the deflection of light from conventional Snell's law, including the frequency-shift enabled by time-refraction and a modulation in the spatial gradient of the refractive index determined by the crossing angle of pump and probe beams. This shows that wavefront shaping is possible not only through fabrication of nanostructures, but can also be engineered all-optically, enabling new forms of transient flat optics. The utilization of pump angle controlled index modulation presents a novel approach to induce a spatial gradient in metamaterials, offering the potential for enhanced effects when combined with nanostructures. Furthermore, the successful demonstration of the ultrafast thin lens serves as compelling evidence of the ability to construct dynamic 2D flat optics by using ENZ materials.

ASSOCIATED CONTENT

Supporting Information

The Supporting Information is available free of charge at https://pubs.acs.org/doi/10.1021/acsphotonics.3c00498.

Additional experimental details and methods, modeling, and simulation details and further experimental results (PDF)

AUTHOR INFORMATION

Corresponding Author

Aaron M. Lindenberg − *Department of Materials Science and Engineering, Stanford University, Stanford, California 94305, United States; Stanford Institute for Materials and Energy Sciences and Stanford PULSE Institute, SLAC National Accelerator Laboratory, Menlo Park, California 94025, United States;* orcid.org/0000-0003-3233-7161; Email: aaronl@stanford.edu

Authors

Qingyuan Fan − *Department of Materials Science and Engineering, Stanford University, Stanford, California 94305, United States;* orcid.org/0000-0001-9137-9017

Amr M. Shaltout − *Geballe Laboratory for Advanced Materials, Stanford University, Stanford, California 94305, United States*

Jorik van de Groep − *Institute of Physics, University of Amsterdam, 1098 XH Amsterdam, The Netherlands;* orcid.org/0000-0003-3033-8005

Mark L. Brongersma − *Department of Materials Science and Engineering, Stanford University, Stanford, California 94305, United States; Geballe Laboratory for Advanced Materials, Stanford University, Stanford, California 94305, United States*

Complete contact information is available at: https://pubs.acs.org/10.1021/acsphotonics.3c00498

Author Contributions

○These authors contributed equally to this work.

Funding

This work was supported by the "Photonics at Thermodynamic Limits" Energy Frontier Research Center funded by the U.S. Department of Energy, Office of Science, Office of Basic Energy Sciences under Award Number DE-SC0019140.

Notes

The authors declare no competing financial interest.

REFERENCES

(1) Lalanne, P.; Astilean, S.; Chavel, P.; Cambril, E.; Launois, H. Design and Fabrication of Blazed Binary Diffractive Elements with Sampling Periods Smaller than the Structural Cutoff. *J. Opt. Soc. Am. A* **1999**, *16* (5), 1143.

(2) Yu, N.; Genevet, P.; Kats, M. A.; Aieta, F.; Tetienne, J.-P.; Capasso, F.; Gaburro, Z. Light Propagation with Phase Discontinuities: Generalized Laws of Reflection and Refraction. *Science* **2011**, *334* (6054), 333−337.

(3) Bomzon, Z.; Biener, G.; Kleiner, V.; Hasman, E. Space-Variant Pancharatnam−Berry Phase Optical Elements with Computer-Generated Subwavelength Gratings. *Opt. Lett.* **2002**, *27* (13), 1141.

(4) Dorrah, A. H.; Capasso, F. Tunable Structured Light with Flat Optics. *Science* **2022**, *376* (6591), na DOI: 10.1126/science.abi6860.

(5) Aieta, F.; Genevet, P.; Kats, M. A.; Yu, N.; Blanchard, R.; Gaburro, Z.; Capasso, F. Aberration-Free Ultrathin Flat Lenses and

Axicons at Telecom Wavelengths Based on Plasmonic Metasurfaces. *Nano Lett.* **2012**, *12* (9), 4932−4936.
(6) Larouche, S.; Tsai, Y. J.; Tyler, T.; Jokerst, N. M.; Smith, D. R. Infrared Metamaterial Phase Holograms. *Nat. Mater.* **2012**, *11* (5), 450−454.
(7) Pors, A.; Bozhevolnyi, S. I. Plasmonic Metasurfaces for Efficient Phase Control in Reflection. *Opt. Express* **2013**, *21* (22), 27438.
(8) Shaltout, A. M.; Shalaev, V. M.; Brongersma, M. L. Spatiotemporal Light Control with Active Metasurfaces. *Science (80-.)* **2019**, *364* (6442), 364.
(9) Liu, G.; Lu, Q.; Guo, W. Ultrafast Speed, Large Angle, and High Resolution Optical Beam Steering Using Widely Tunable Lasers. *OSA Contin* **2019**, *2* (5), 1746.
(10) Heck, M. J. R. Highly Integrated Optical Phased Arrays: Photonic Integrated Circuits for Optical Beam Shaping and Beam Steering. *Nanophotonics* **2017**, *6* (1), 93−107.
(11) Jarrahi, M.; Fabian, R.; Pease, W.; Miller, D. A. B.; Lee, T. H. High-Speed Optical Beam-Steering Based on Phase-Arrayed Waveguides. *J. Vac. Sci. Technol. B Microelectron. Nanom. Struct.* **2008**, *26* (6), 2124−2126.
(12) Wu, P. C.; Pala, R. A.; Kafaie Shirmanesh, G.; Cheng, W. H.; Sokhoyan, R.; Grajower, M.; Alam, M. Z.; Lee, D.; Atwater, H. A. Dynamic Beam Steering with All-Dielectric Electro-Optic III−V Multiple-Quantum-Well Metasurfaces. *Nat. Commun.* **2019**, *10* (1), 1−9.
(13) Andersen, T. I.; Gelly, R. J.; Scuri, G.; Dwyer, B. L.; Wild, D. S.; Bekenstein, R.; Sushko, A.; Sung, J.; Zhou, Y.; Zibrov, A. A.; Liu, X.; Joe, A. Y.; Watanabe, K.; Taniguchi, T.; Yelin, S. F.; Kim, P.; Park, H.; Lukin, M. D. Spatial Light Modulation at the Nanosecond Scale with an Atomically Thin Reflector. *arXiv:2111.04781 [cond-mat.mes-hall]* **2021**, na.
(14) Tuantranont, A.; Bright, V. M.; Zhang, J.; Zhang, W.; Neff, J. A.; Lee, Y. C. Optical Beam Steering Using MEMS-Controllable Microlens Array. *Sensors Actuators, A Phys.* **2001**, *91* (3), 363−372.
(15) Ferdinandus, M. R.; Hu, H.; Reichert, M.; Hagan, D. J.; Van Stryland, E. W. Beam Deflection Measurement of Time and Polarization Resolved Nonlinear Refraction. *Opt. InfoBase Conf. Pap.* **2013**, *38* (18), 3518−3521.
(16) Li, Y.; Chen, D. Y.; Yang, L.; Alfano, R. R. Ultrafast All-Optical Deflection Based on an Induced Area Modulation in Nonlinear Materials. *Opt. Lett.* **1991**, *16* (6), 438.
(17) Mendonca, J T; Shukla, P K Time Refraction and Time Reflection: Two Basic Concepts. *Phys. Scr.* **2002**, *65*, 160−163.
(18) Bohn, J.; Luk, T. S.; Horsley, S.; Hendry, E. Spatiotemporal Refraction of Light in an Epsilon-near-Zero ITO Layer. *Optica* **2021**, *8*, 1532.
(19) Bhaduri, B.; Yessenov, M.; Abouraddy, A. F. Anomalous Refraction of Optical Spacetime Wave Packets. *Nat. Photonics* **2020**, *14* (7), 416−421.
(20) Zhou, Y.; Alam, M. Z.; Karimi, M.; Upham, J.; Reshef, O.; Liu, C.; Willner, A. E.; Boyd, R. W. Broadband Frequency Translation through Time Refraction in an Epsilon-near-Zero Material. *Nat. Commun.* **2020**, *11* (1), na DOI: 10.1038/s41467-020-15682-2.
(21) Shcherbakov, M. R.; Werner, K.; Fan, Z.; Talisa, N.; Chowdhury, E.; Shvets, G. Photon Acceleration and Tunable Broadband Harmonics Generation in Nonlinear Time-Dependent Metasurfaces. *Nat. Commun.* **2019**, *10* (1), 1−9.
(22) Khurgin, J. B.; Clerici, M.; Bruno, V.; Caspani, L.; DeVault, C.; Kim, J.; Shaltout, A.; Boltasseva, A.; Shalaev, V. M.; Ferrera, M.; Faccio, D.; Kinsey, N. Adiabatic Frequency Shifting in Epsilon-near-Zero Materials: The Role of Group Velocity. *Optica* **2020**, *7* (3), 226.
(23) Carnemolla, E. G.; Bruno, V.; Caspani, L.; Clerici, M.; Vezzoli, S.; Roger, T.; DeVault, C.; Kim, J.; Shaltout, A.; Shalaev, V.; Boltasseva, A.; Faccio, D.; Ferrera, M. Giant Nonlinear Frequency Shift in Epsilon-near-Zero Aluminum Zinc Oxide Thin Films. *CLEO 2018* **2018**, SM4D.7.
(24) Shaltout, A. M.; Clerici, M.; Kinsey, N.; Kaipurath, R.; Kim, J.; Carnemolla, E. G.; Faccio, D.; Boltasseva, A.; Shalaev, V. M.; Ferrera, M. Doppler-Shift Emulation Using Highly Time-Refracting TCO Layer. *Conf. Lasers Electro-Optics; CLEO 2016*, San Jose, CA, June 5−10, 2016, Optica Publishing Group, 2016; pp 6−7. DOI: 10.1364/cleo_qels.2016.ff2d.6.
(25) Vezzoli, S.; Bruno, V.; Devault, C.; Roger, T.; Shalaev, V. M.; Boltasseva, A.; Ferrera, M.; Clerici, M.; Dubietis, A.; Faccio, D. Optical Time Reversal from Time-Dependent Epsilon-Near-Zero Media. *Phys. Rev. Lett.* **2018**, *120* (4), 43902.
(26) Shaltout, A.; Kildishev, A.; Shalaev, V. Time-Varying Metasurfaces and Lorentz Non-Reciprocity. *Opt. Mater. Express* **2015**, *5* (11), 2459.
(27) Hadad, Y.; Sounas, D. L.; Alu, A. Space-Time Gradient Metasurfaces. *Phys. Rev. B - Condens. Matter Mater. Phys.* **2015**, *92* (10), 1−6.
(28) Nozaki, K.; Tanabe, T.; Shinya, A.; Matsuo, S.; Sato, T.; Taniyama, H.; Notomi, M. Sub-Femtojoule All-Optical Switching Using a Photonic-Crystal Nanocavity. *Nat. Photonics* **2010**, *4* (7), 477−483.
(29) Berini, P. Optical Beam Steering Using Tunable Metasurfaces. *ACS Photonics* **2022**, *9* (7), 2204−2218.
(30) Alam, M. Z.; De Leon, I.; Boyd, R. W. Large Optical Nonlinearity of Indium Tin Oxide in Its Epsilon-near-Zero Region. *Science (80-.)* **2016**, *352* (6287), 795−797.
(31) Reshef, O.; De Leon, I.; Alam, M. Z.; Boyd, R. W. Nonlinear Optical Effects in Epsilon-near-Zero Media. *Nat. Rev. Mater.* **2019**, *4* (8), 535−551.
(32) Park, J.; Kang, J. H.; Liu, X.; Brongersma, M. L. Electrically Tunable Epsilon-Near-Zero (ENZ) Metafilm Absorbers. *Sci. Rep.* **2015**, *5* (Mim), 1−9.
(33) Mendonça, J. T. Nonlinear Interaction of Wave Packets. *J. Plasma Phys.* **1979**, *22* (1), 15−26.
(34) Gavrilenko, V. G.; Stepanov, N. S. Transformation of the Wave Spectrum in a Medium Having Smooth Space-Time Fluctuations. *Radiophys. Quantum Electronics* **1973**, *16*, 50.
(35) Quéré, F.; Vincenti, H.; Borot, A.; Monchocé, S.; Hammond, T. J.; Kim, K. T.; Wheeler, J. A.; Zhang, C.; Ruchon, T.; Auguste, T.; Hergott, J. F.; Villeneuve, D. M.; Corkum, P. B.; Lopez-Martens, R. Applications of Ultrafast Wavefront Rotation in Highly Nonlinear Optics. *J. Phys. B At. Mol. Opt. Phys.* **2014**, *47* (12), 124004.
(36) Estakhri, N. M.; Alù, A. Wave-Front Transformation with Gradient Metasurfaces. *Phys. Rev. X* **2016**, *6* (4), 041008.
(37) Yu, N.; Genevet, P.; Kats, M. a.; Aieta, F.; Tetienne, J.-P.; Capasso, F.; Gaburro, Z. Light Propagation with Phase Reflection and Refraction. *Science* **2011**, *334* (6054), 333−337.
(38) Naik, G. V.; Shalaev, V. M.; Boltasseva, A. Alternative Plasmonic Materials: Beyond Gold and Silver. *Adv. Mater.* **2013**, *25* (24), 3264−3294.
(39) Kelley, P. L. Self-Focusing of Optical Beams. *Phys. Rev. Lett.* **1965**, *15*, 1005.
(40) Marburger, J. H. *SELF-FOCUSING: THEORY*; Pergamon Press, 1975; Vol. *4*. DOI: 10.1016/0079-6727(75)90003-8.
(41) Shen, Y. R. Self-Focusing: Experimental. *Prog. Quantum Electron.* **1975**, *4*, 1−34.
(42) Saha, S.; Segal, O.; Fruhling, C.; Lustig, E.; Segev, M.; Boltasseva, A.; Shalaev, V. M. Photonic time crystals: a materials perspective. *Opt. Express* **2023**, *31* (5), 8267.
(43) Hayran, Z.; Khurgin, J. B.; Monticone, F. $\hbar\omega$ versus $\hbar$k: dispersion and energy constraints on time-varying photonic materials and time crystals [Invited]. *Optical Materials Express* **2022**, *12* (10), 3904.
(44) Tirole, R.; Vezzoli, S.; Galiffi, E.; Robertson, I.; Maurice, D.; Tilmann, B.; Maier, S. A.; Pendry, J. B.; Sapienza, R. Double-slit time diffraction at optical frequencies. *Nat. Phys.* **2023**, DOI: 10.1038/s41567-023-01993-w.

https://doi.org/10.1021/acsphotonics.3c00498
ACS Photonics XXXX, XXX, XXX−XXX